

Electronic Supplementary Material (ESI) for ChemComm.
This journal is © The Royal Society of Chemistry 2015

Supporting Information

Graphene Modified Mesoporous Titania Single Crystals with Controlled and Selective Photoredox Surfaces

*Yi Zhou,^a Qiuying Yi,^a Mingyang Xing,^{*a} Lu Shang,^b Tierui Zhang,^{*b} and Jinlong Zhang^{*a}*

^aKey Laboratory for Advanced Materials and Institute of Fine Chemicals, East China University of Science and Technology, 130 Meilong Road, Shanghai 200237, P.R. China
E-mail: mingyangxing@ecust.edu.cn; jlzhang@ecust.edu.cn
Tel: +86-21-64252062

^bKey Laboratory of Photochemical Conversion and Optoelectronic Materials Technical Institute of Physics and Chemistry, Chinese Academy of Sciences, Beijing 100190, P.R. China
Tel: +86-10-82543428
Fax: +86-10-62554670
E-mail: tierui@mail.ipc.ac.cn

Part S1. Experimental sections

Preparation of SiO₂ spheres. The silica spheres were synthesized by the Stöber method.¹ 167.2 mL absolute ethanol was mixed with 28.8 mL water and 4.0 mL ammonium hydroxide solution in a beaker. The mixture was stirred for 1 min at room temperature. Simultaneously, 18.0 mL tetraethoxysilane (TEOS) was mixed with 182.0 mL absolute ethanol at room temperature. The TEOS solution was stirred for 1 min, and then was poured into the above mentioned mixture. The precursor liquid was stirred for 24 h to obtain a suspension which is the silica colloids.

Preparation of graphene embedded silica templates. The graphene oxides (GOs) were prepared by a modified hummers method.^{2, 3} 400.0 mL silica colloids were mixed with 40.0 mL graphene oxide solution (1.0 mg/mL), and the mixture was ultrasonic for 12 h to afford an emulsion with a uniform earthy yellow color. The emulsion was centrifuged at a high speed (13000 r.p.m) to obtain a cyaneous solid. The solid was dried at 60 °C for 12 h and calcinated at 500 °C for 2 h in the vacuum to obtain the graphene embedded silica templates. The graphene modified templates were denoted as GR-SiO₂. The pure silica templates without graphene were prepared by the same method in the absence of graphene oxides.

Preparation of TiO₂ seeded silica templates. 7.0 g graphene embedded silica templates of GR-SiO₂ were immersed into 30 mL TiCl₄ solution (0.05 M) at 70 °C for 1 h, followed by several washes using water. The solids were dried at 60 °C in the vacuum for 12 h. The dried templates were calcinated at 500 °C in the vacuum for 2h. The seeded templates with graphene were denoted as GR-Ti-SiO₂. The TiO₂ seeded silica templates without graphene was prepared by using the pure silica templates via a same procedure, which was denoted as Ti-SiO₂.

Preparation of sandwich structured graphene modified mesoporous TiO₂ single crystals. 14.0 mL water was mixed with 14.0 mL HCl and stirred for 10 min at the room temperature. 0.4 mL tetrabutyltitanate (TBOT) and 15.0 μL HF were added into the solution in sequence and stirred for another 10 min. 0.4 g GR-Ti-SiO₂ templates were added in the solution and removed to a teflon-inner-linear stainless steel autoclave, which was kept under 453 K for 12 h. The obtained powders was washing with NaOH solution at 80 °C for 1 h to etch the SiO₂ templates. After the corrosion, the powders were washed with water and ethanol for several times and dried at 60 °C for 12 h, which were denoted as GR-MSCs (the schematic illustration is shown in Scheme 1). GR-MSCs(2) and GR-MSCs(0.5) were prepared with 80.0 mL graphene oxide solution (1.0 mg/mL) and 20.0 mL graphene oxide solution (1.0 mg/mL),

respectively. The blank TiO₂ MSCs were prepared by the same method in the absence of graphene and by using the Ti-SiO₂ as the precursor.

Preparation of core-shell structured graphene modified mesoporous TiO₂ single crystals. 10 mL graphene oxides (1.0×10^{-4} mg/l) was added into a solution of 0.1 g blank TiO₂ MSCs mixed with 50 mL water. The solution was dispersed by ultrasonic and continuous bubbling of CO₂ for 3 hours. The powders were collected by the centrifugation and freeze dried. The core-shell structured graphene modified MSCs were denoted as MSCs@GR. And the core-shell structured graphene modified TiO₂ single crystals with different amount of graphene were also synthesized, using using 20 mL graphene oxides (1.0×10^{-4} mg/l) for MSCs@GR(2) and 5 mL graphene oxides (1.0×10^{-4} mg/l) for MSCs@GR(0.5), respectively. The Schematic illustration of the growth pathways of MSCs@GR is shown in Scheme 1. The core-shell structured TiO₂@graphene composite was prepared by the same ultrasonic-bubbling method, and the preparation of TiO₂ solid single crystals were according to the previous work.⁴

Characterization. X-ray diffraction measurements (XRD) were performed with a Rigaku Ultima IV (Cu K α radiation, $\lambda = 1.5406 \text{ \AA}$) in the range of 10-80° (2 θ). The morphologies were characterized by transmission electron microscopy (TEM, JEM2100) and field emission scanning electron microscopy (FESEM, Nova Nano SEM 450). The instrument employed for X-ray photoelectron spectroscopy (XPS) studies was a Perkin-Elmer PHI 5000C ESCA system with Al K α radiation. The shift of the binding energy was referenced to the C1s level at 284.6 eV as an internal standard. The Raman spectra measurements were recorded with an in Via Reflex Raman spectrometer with 524.5 nm laser excitation. UV-vis diffuse reflectance spectra (DRS) were obtained with a SHIMADZU UV-2600 spectroscope equipped with an integrating sphere assembly and using BaSO₄ as reflectance sample. BET specific surface area measurements were carried out by N₂ adsorption at 77 K using an ASAP2020 instrument. Thermogravimetric and differential thermal analyses were conducted on a Pyris Diamond TG/DTA (PerkinElmer) apparatus at a heating rate of 20 K min⁻¹ from 40 to 800 °C in air flow. The photoluminescence (PL) emission spectra of the solid catalysts were also measured using luminescence spectrometry (Cary Eclipse) at room temperature under the excitation light at 350 nm. All the electrochemical experiments included electro-chemical impedance spectroscopy and photocurrents measurements were carried out on an electrochemical analyzer (CHI 660 D electrochemical station, CHI Instruments Inc.) at room temperature. A standard three-electrode system consisting of a working electrode (as-prepared samples as the working electrodes with an active area of ca. 0.5 cm²), a Pt wire as the counter electrode and

a saturated Ag/AgCl as the reference electrode was employed. Transient photocurrent responses of different samples were carried out in 0.5 M Na₂SO₄ aqueous solution under various irradiation conditions (300 W Xe lamp). The EIS measurements were performed in the presence of a 2.0 mM K₃[Fe(CN)₆] and 0.5 M KCl mixture aqueous solution. Fourier transform infrared (FTIR) spectra were recorded with KBr disks containing the powder sample with the FTIR spectrometer (Nicolet Magna 550).

Detection of photogenerated holes. The number of photo-generated holes were detected by the indirect measurement of •OH in a terephthalic acid solution. 0.01 g of catalyst was mixed with 20 mL of terephthalic acid (5×10^{-4} M) and sodium hydroxide (2×10^{-3} M) solution. The mixture was irradiated under light irradiation (300 W Xe lamp) for 30 min. The solution was filtered and the filtrate was studied by PL emission spectroscopy to indirectly measure the amount of •OH produced (excitation wavelength: 315 nm).

Detection of photogenerated electrons. The number of photo-generated electrons is detected by the indirect measurement of Fe²⁺ in a Fe³⁺ solution. 0.01 g of the catalyst was mixed with 20 mL of Fe³⁺ solution which contains 12.0 mL ammonium ferric sulfate (2.0×10^{-5} M), 5.0 mL buffered solution (acetic acid/sodium acetate) and 3.0 mL 1, 10-phenanthroline monohydrate (0.1 wt%, Phen). The mixture was irradiated under light (300 W Xe lamp) for 60 min. The solution was filtered and the filtrate was studied by using a Cary 100 ultraviolet visible spectrometer.

Photocatalytic oxidation of phenol. The photo-catalyst (0.05 g) was added into a 100 mL quartz photoreactor containing 50 mL of a phenol solution (10 mg/l). The mixture was stirred for 120 min in the dark in order to reach the adsorption–desorption equilibrium. A 300 W Xe lamp with an AM 1.5 air mass filter was used as a simulated solar light source. At the given time intervals, the analytical samples were taken from the mixture and immediately centrifuged, then filtered through a 0.22 μm Millipore filter to remove the photo-catalysts. The filtrates were analyzed by a CTO-10 ASVP high-performance liquid chromatograph.

Water splitting for H₂ generation. Photo-catalytic H₂ generation experiments were carried out in a sealed circulation system. 0.10 g of sample was suspended in 100 mL 20% methanol aqueous solution (containing 1 mL H₂PtCl₆, 1 g/L) under magnetic stirring. Then the above solution was irradiated under a 300 W Xe lamp (with an AM 1.5 air mass filter) for 180 minutes, which resulted in the loading of Pt nanoparticles on the surface of the catalyst (0.377 wt% Pt). The photo-catalytic H₂ generation activities of sandwich and core-shell structured graphene modified mesoporous TiO₂ single crystals in the absence of Pt nanoparticles and different amounts of Pt loading were also tested. After degassing the system, the photo-

catalytic reaction was executed, and the products were analyzed by gas chromatography (Techcomp GC-7890II) equipped with a thermal conductivity detector (TCD).

Part S2. Characterization of photo-catalysts

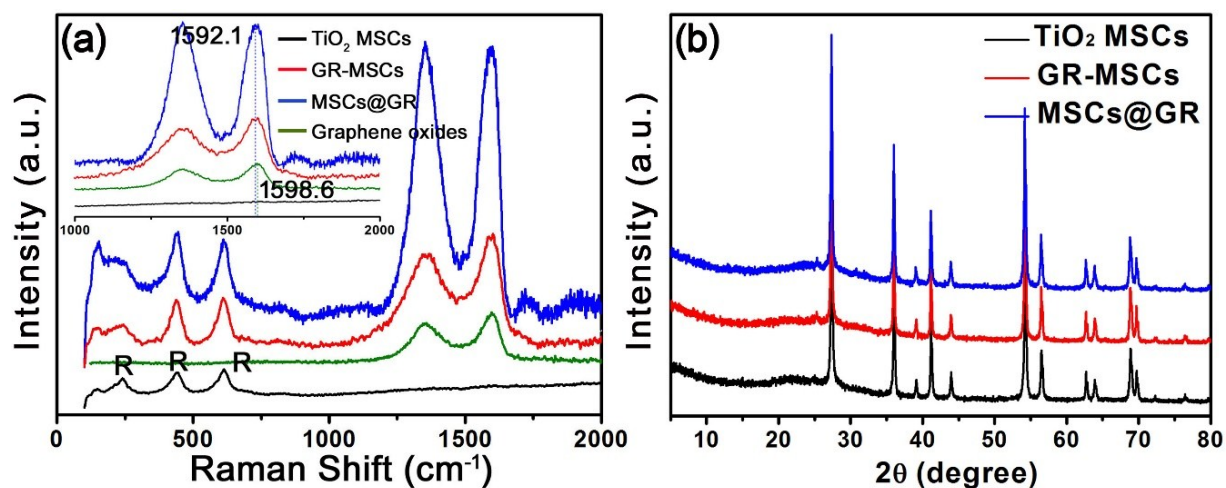


Fig. S1 (a) Raman spectra of different graphene modified TiO₂ MSCs. Inset is the amplification of D and G band. (b) XRD spectra of different graphene modified TiO₂ MSCs.

The presence of HCl in the preparation promotes the generation of rutile.^{5,6} The G-bands of the Raman spectra at 1598.6 cm⁻¹ shift to 1592.1 cm⁻¹, indicating the successful reduction of GO by GR-MSCs and MSCs@GR.⁷ The increased intensity ratio of the D/G bands in the graphene-modified MSCs further confirms the reduction of GO.⁸

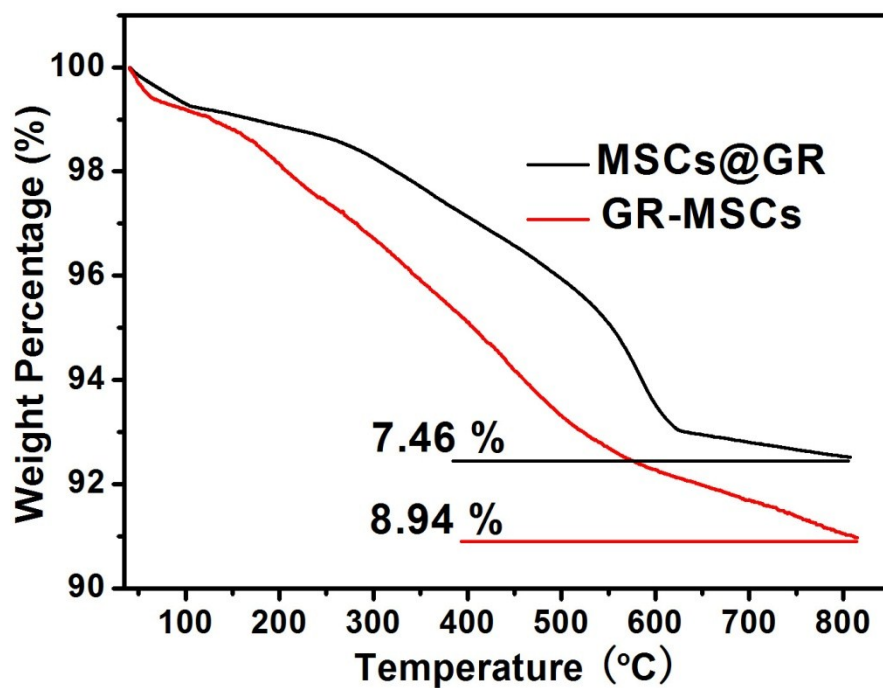


Fig. S2 TG spectra of different graphene modified TiO₂ MSCs.

Using these methods, weight losses of approximately 8.94 % and 7.46 % were observed, indicating that the proportions of graphene in GR-MSCs and MSCs@GR are 8.94 % and 7.46 %, respectively.

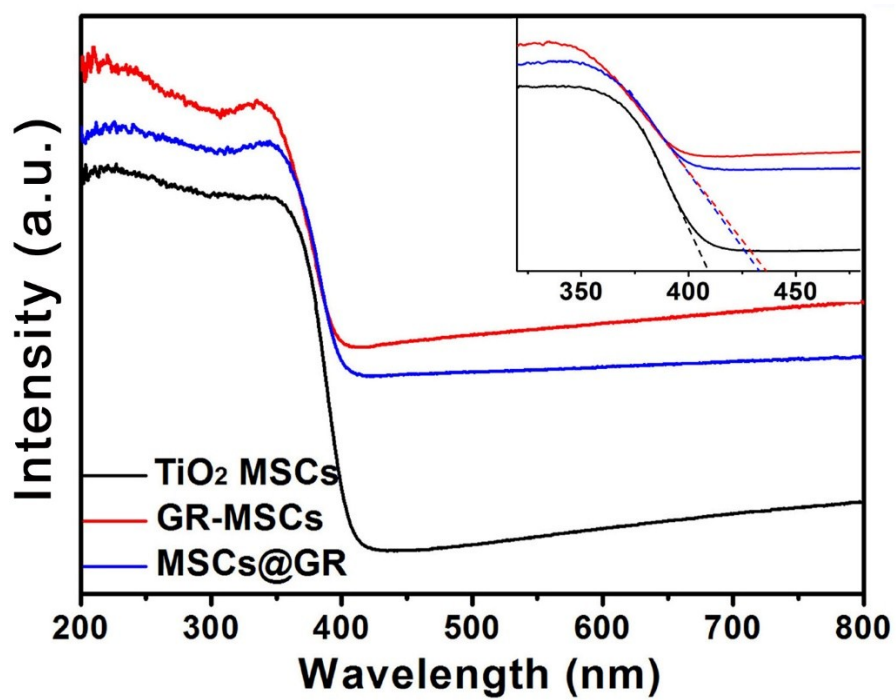


Fig. S3 UV-vis DRS spectra of different graphene modified TiO₂ MSCs.

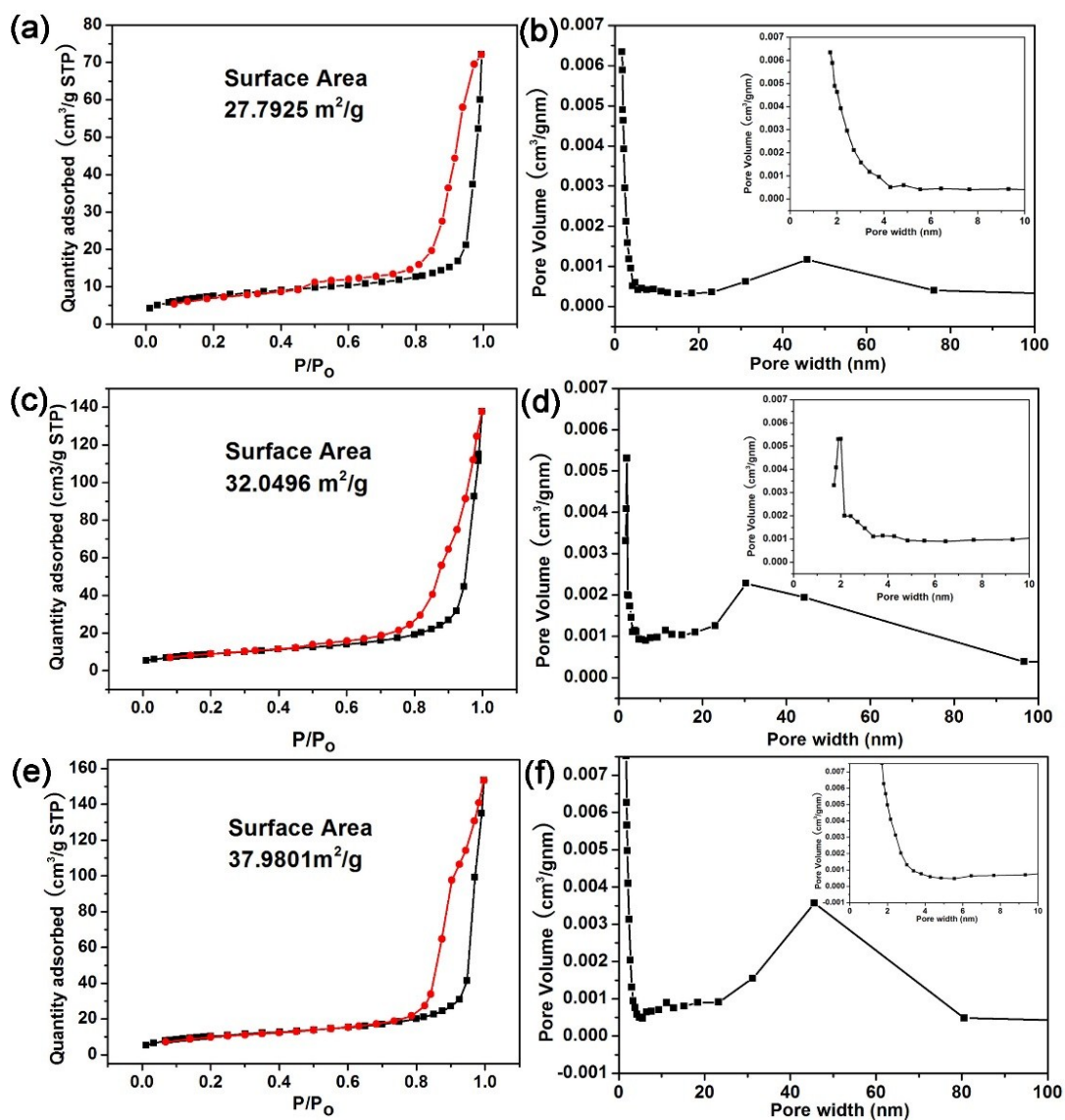


Fig. S4 Nitrogen adsorption-desorption isotherms and the corresponding pore size distribution curves. TiO₂ MSCs (a, b), GR-MSCs (c, d) and MSCs@GR (e, f).

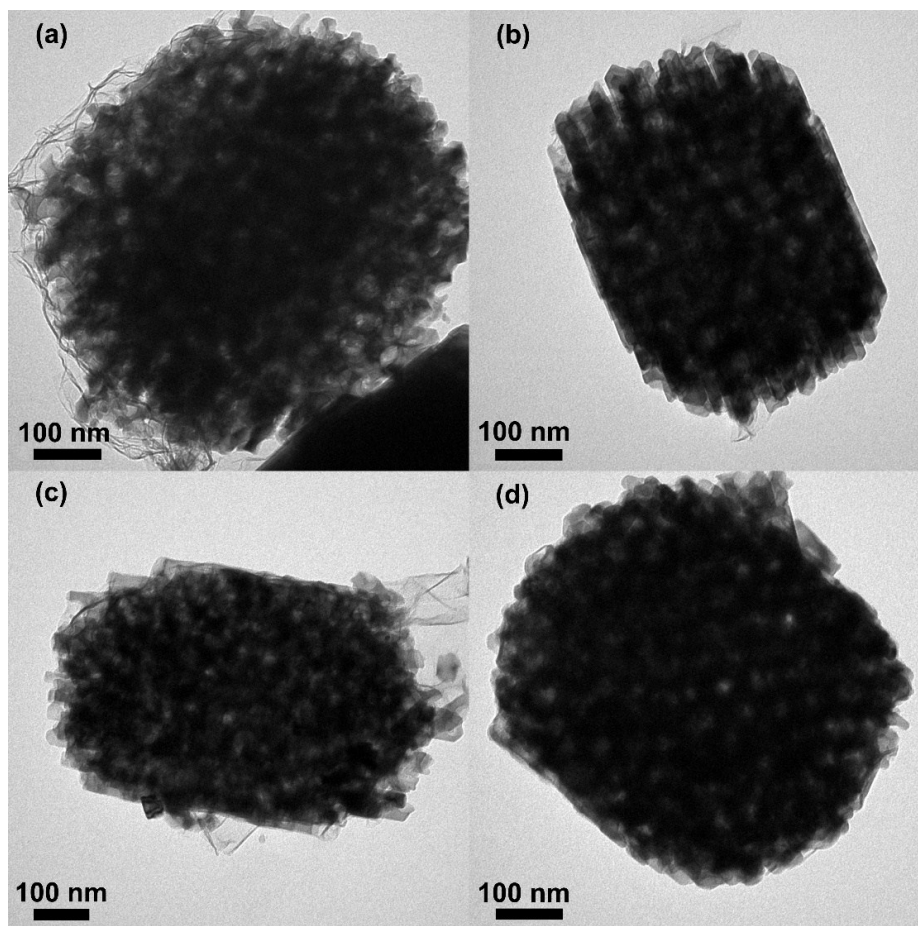


Fig. S5 TEM images of (a) GR-MSCs(2), (b) GR-MSCs(0.5), (c) MSCs@GR(2) and (d) MSCs@GR(0.5).

Compared with GR-MSCs, the edges of GR-MSCs(2) appear clearly rough because a lot of fringes of sandwiched graphene are exposed on the surface. On the contrary, the edges of GR-MSCs(0.5) appear slightly rough because a few fringes of sandwiched graphene are exposed on the surface. With increasing amount of graphene in MSCs@GR, thickness of graphene coated on the surface of MSCs increased (**Fig. S4**). TEM images confirmed that the TiO₂ MSCs were firmly encapsulated by graphene sheets even after the composites were under strong ultrasonic treatment for 3h in order to enable TEM characterization.

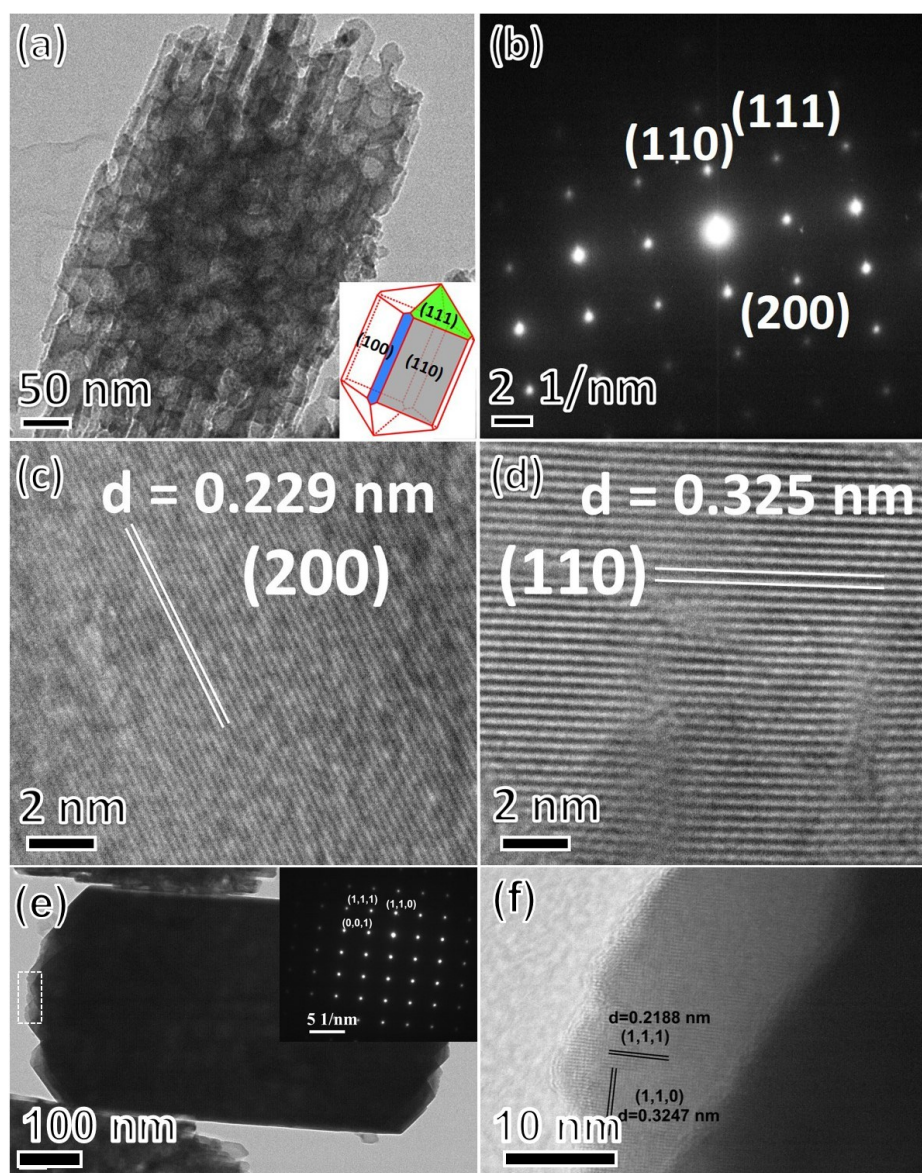


Fig. S6 TEM image (a) and the corresponding SAED pattern (b) recorded for the whole particle of GR-MSCs. (c, d) Corresponding high resolution TEM image recorded for the GR-MSCs. Inset of (a) is the shape model of a rutile crystal. (e) TEM image and SAED pattern of the TiO₂ MSCs. (f) HRTEM image for the amplification of the square frame in (e).

In order to further demonstrate the synthesized MSCs is indeed the mesoporous single crystal, the TEM image with proper magnificence was given in Fig. S6e,f to reveal the interface information on MSCs. There is an obvious regular block appearance in Fig. S6e and the corresponding SAED patterns shown in the insets display the single crystalline nature of the prepared TiO₂ MSCs. The diffraction lattice matrix of (110) in Fig. S6e is parallel with the {110} facets and vertical with the diffraction lattice matrix of (001), which indicates the TiO₂ prefers to form a [001]-oriented tetragonal rutile single crystal with dominant {110} facets, owing to the working of HCl to lower the activation energy for the rutile formation. The

amplification of the fringe of single crystal in Fig. S6e are shown in Fig. S6f. There is no grain boundary and all the lattice fringes are long-term orderly arrangement, indicating the single crystalline nature of TiO_2 MSCs. The vertical lattice fringes of (110) and (111) also verify the dominant exposing of {110} facets on TiO_2 MSCs.

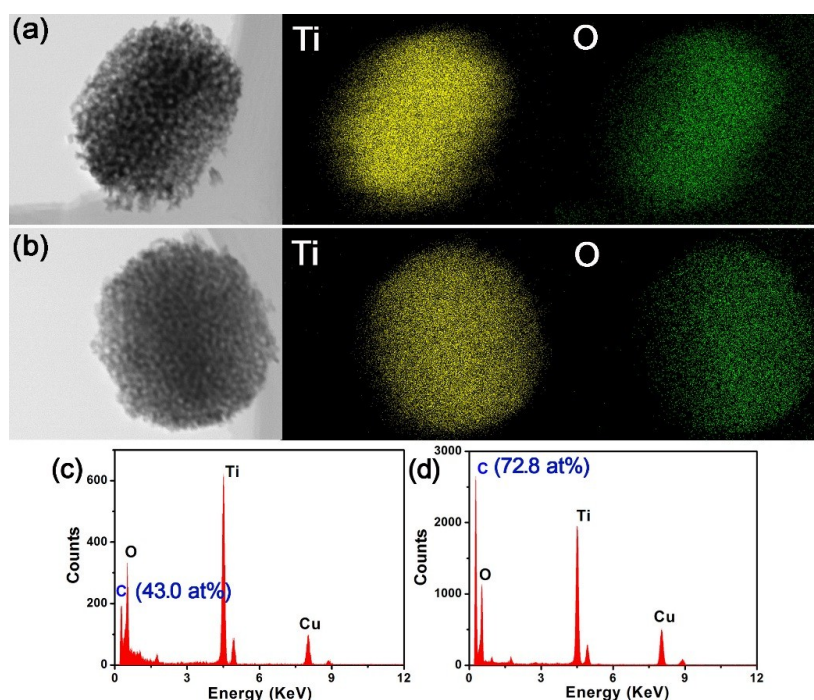


Fig. S7 TEM image and the corresponding Ti and O element mapping images. (a) TiO_2 MSCs, (b) GR-MSCs. The corresponding carbon concentrations of (c) TiO_2 MSCs and (d) GR-MSCs.

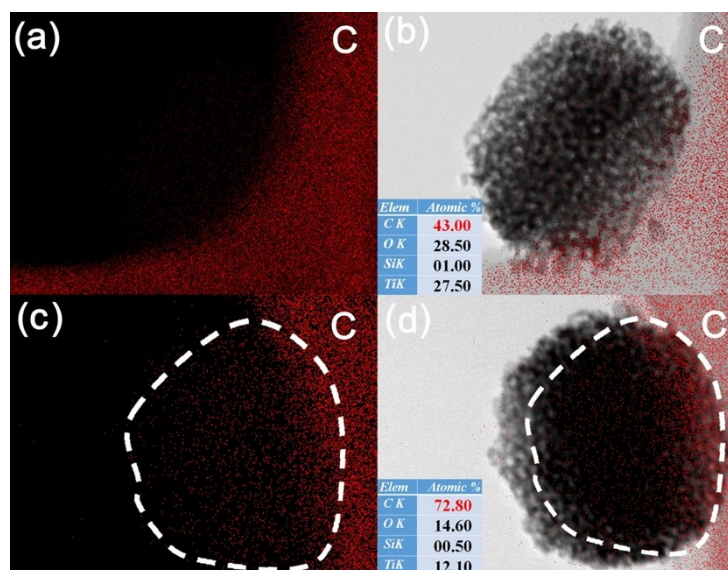


Fig. S8 Carbon element mapping image and the corresponding carbon concentration of (a, b) TiO_2 MSCs, (c, d) GR-MSCs.

The element mapping images of TiO_2 MSCs and GR-MSCs presented in Fig. S6 and Fig. S7 confirm the presence of sandwich structured GR-MSCs. The distribution profiles of Ti and O elements in the TEM map are consistent with the profile of the MSC (Fig. S6a,b), verifying that the mesoporous particle is a TiO_2 single crystal. The C element in the TEM map of pure TiO_2 MSC suggests that the concentration of carbon in the bulk of blank TiO_2 is very low. The calculated percentage of 43.0 at% is mostly accounted for by the carbon coated on the

Lacey support film (Fig. S6c and Fig. S7a,b). There is no visible C element present in the bulk of the TiO₂ MSCs, as indicated by the red dots in Fig. S7a,b. The majority of the visible red dots are limited to the support film. However, when graphene has been introduced into the bulk of the TiO₂ MSCs, many clearly distinguishable red dots appear in the region corresponding to the bulk of the MSCs. (Fig. S7c,d). The C concentration also increases to 72.8 at%, further indicating the new presence of C atoms in the MSCs. The absence of carbon at the edges of the GR-MSCs indicates that the graphene is indeed embedded inside the MSC, affording a sandwich-like structure.

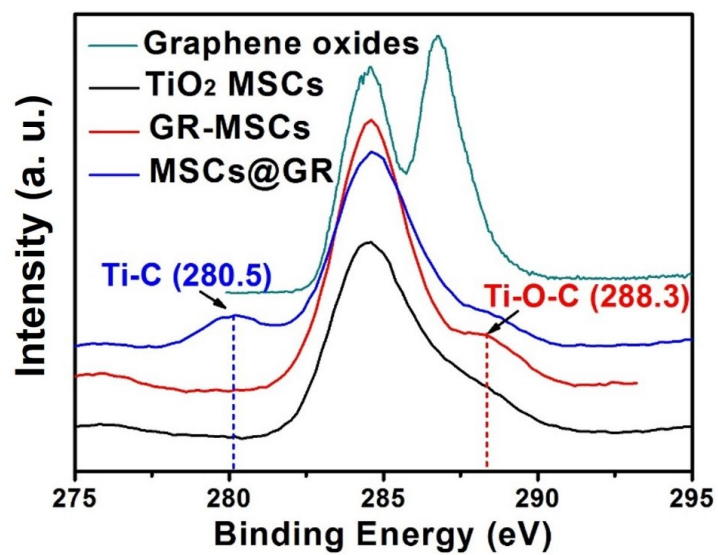


Fig. S9 Chemical environment between graphene and TiO₂ MSCs. C1s XPS spectra for the pure graphene oxides and graphene modified MSCs.

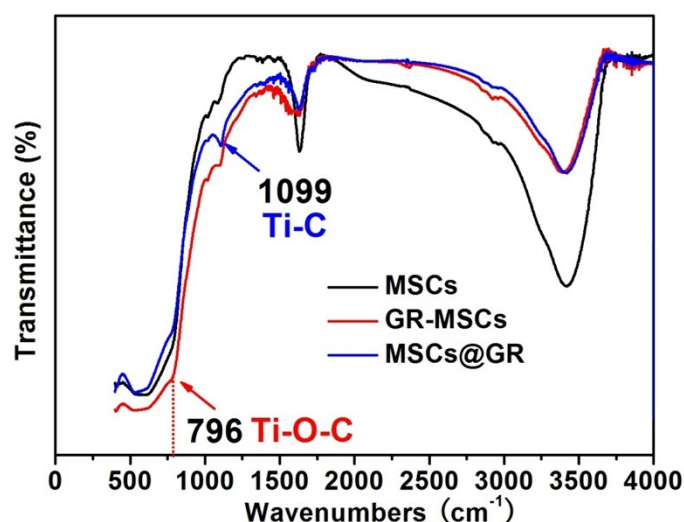


Fig. S10 FTIR spectra of different samples.

The XPS and FTIR spectra in Fig. S8 and S9 shed light on the catalytic effect of graphene in the systems investigated here. Compared with the C1s XPS spectrum of graphene oxides (Fig. S8), the characteristic peaks of C-OH, C-O-C, and OH-C=O at 285.0~288.0 eV all decrease significantly in the presence of GR-MSCs and MSCs@GR, indicating the extensive reduction of graphene oxides.^{9, 10} Compared to the reaction using blank TiO₂ MSCs, the use of sandwiched GR-MSCs affords a new peak at 288.3 eV resulting from the generation of Ti-O-C bonds between graphene and MSCs.^{10, 11} During the growth of TiO₂ seeds, the surface -OH groups on graphene are easily bound to the surface -OH of the TiO₂ crystal seeds, resulting in formation of Ti-O-C bonds. These chemical bonds firmly embed the graphene sheets into the bulk of TiO₂ MSC. As the MSC grows, the graphene is sandwiched into the middle of the TiO₂. When the graphene is wrapped around the surface of TiO₂ using an ultrasonic-bubbling treatment, the expected Ti-C bonds between TiO₂ and graphene are observed as indicated by the peaks appearing at 280.5 eV.¹²⁻¹⁴ The ultrasonic treatment is strong enough to generate surface chemical bonds between graphene and TiO₂.¹⁰ The FTIR results further confirm the interaction of TiO₂ with graphene (Fig. S9). The small peaks at 796 cm⁻¹ and 1099 cm⁻¹ are assigned to Ti-O-C bonds and Ti-C bonds, respectively.^{15, 16} These chemical bonds assist in narrowing the bandgap of TiO₂, thus affording the photocatalytic activity of GR-MSCs and MSCs@GR achievable under solar light irradiation.^{16, 17}

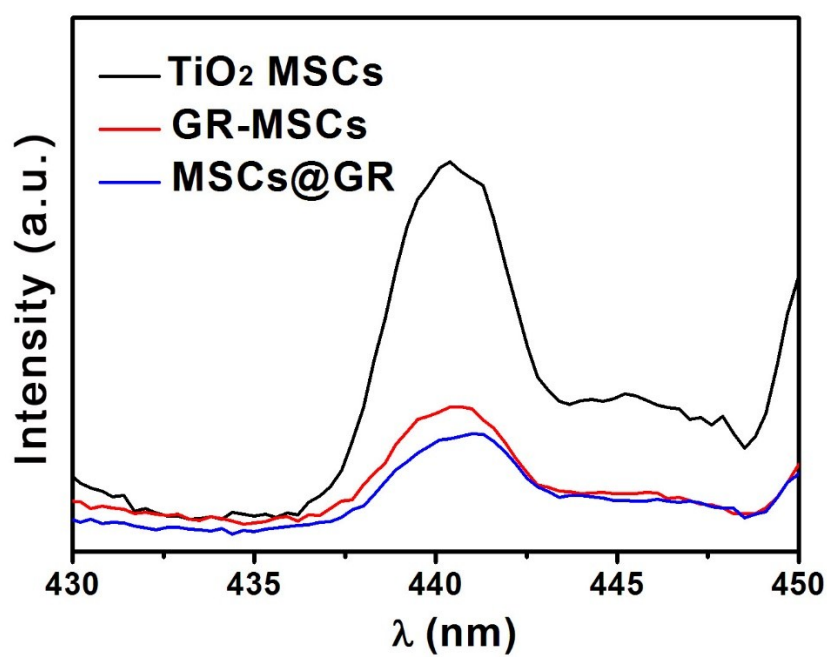


Fig. S11 PL spectra of different powder photo-catalysts (excitation wavelength: 350 nm).

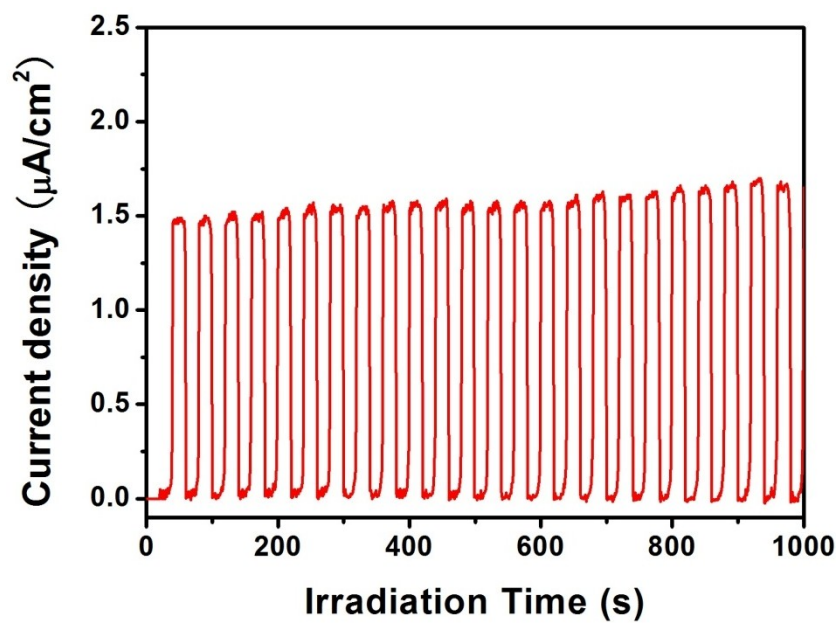


Fig. S12 Transient photocurrent responses of sandwiched GR-MSCs under the light irradiation for 1000 s (300 W Xe lamp).

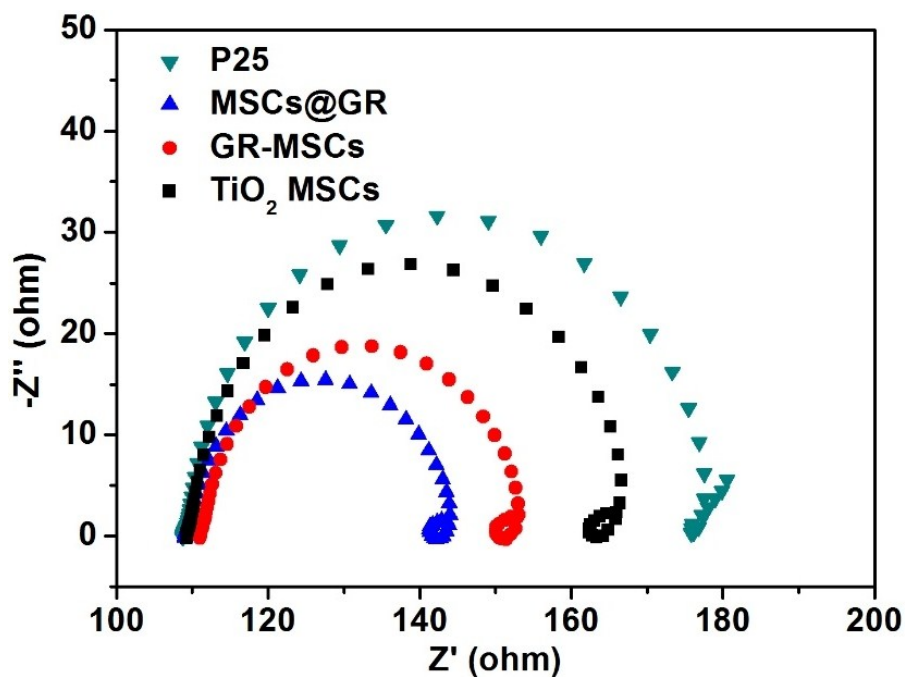


Fig. S13 EIS changes of different samples under irradiation (The EIS measurements were performed in the presence of a 2.0 mM $K_3[Fe(CN)_6]$ and 0.5 M KCl mixture aqueous solution.)

The impedance of sandwiched and core-shell structured graphene modified mesoporous TiO_2 single crystals are much lower compared with that of blank TiO_2 MSCs and P25. It is clear that the size of the arc radius on the EIS Nyquist plot is reduced due to the photo-irradiation. It indicated that reaction rate occurring at electrode surface increased under irradiation.¹⁸

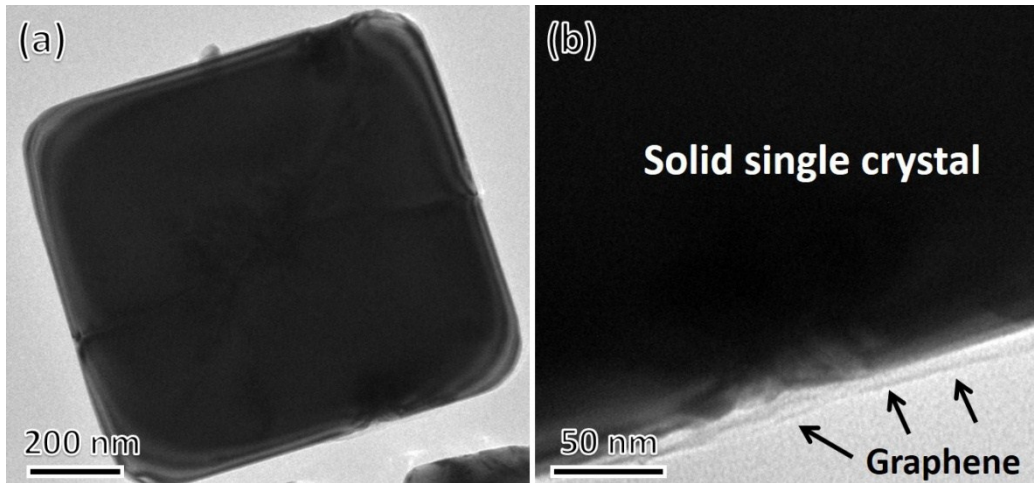


Fig. S14 (a, b)TEM images for the core-shelled graphene modified the solid TiO_2 single crystal (solid TiO_2 @graphene).

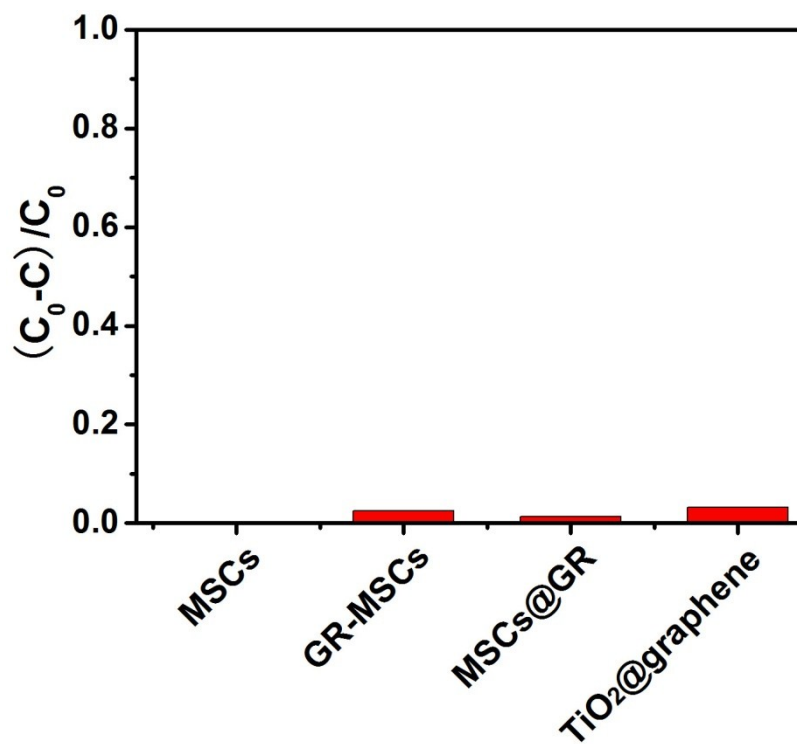


Fig. S15 Adsorption capacity for phenol on different samples in the dark.

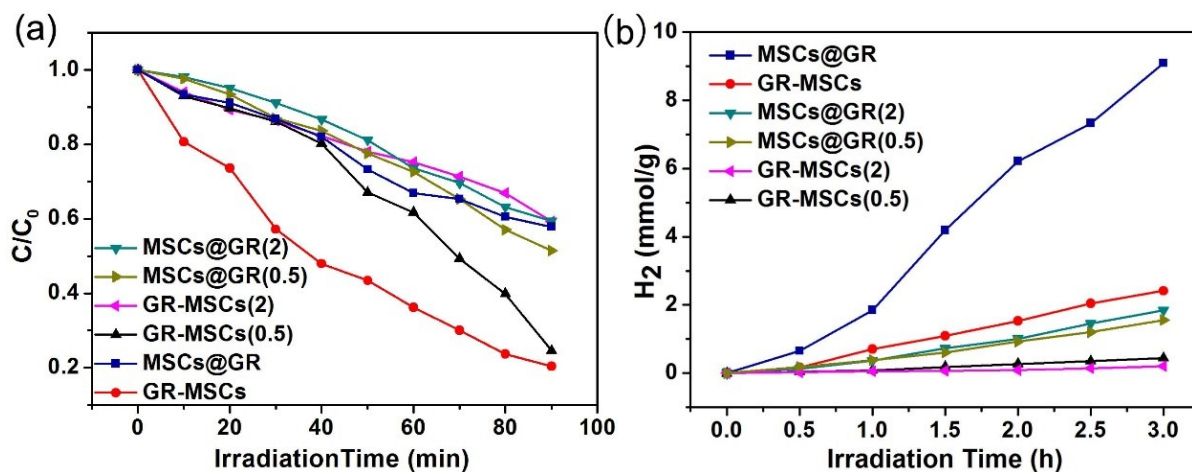


Fig. S16 Photocatalytic activity of sandwich and core-shell structured graphene modified mesoporous TiO₂ single crystals with increased and decreased graphene content. (a) Photo-oxidation activities for phenol degradation induced by simulated solar light (with an AM 1.5 air mass filter). (b) Solar light driven (with an AM 1.5 air mass filter) photo-catalytic water reduction for H₂ generation.

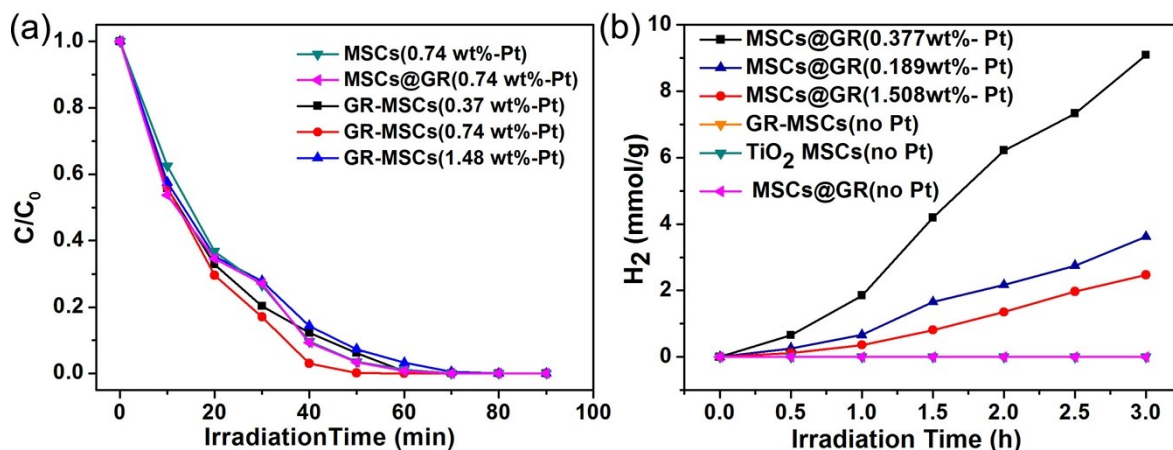


Fig. S17 (a) Photo-oxidation activities on GR-MSCs loaded with different amount of Pt, MSCs and MSCs@GR with 0.74 wt% Pt for phenol degradation under simulated solar light (with an AM 1.5 air mass filter). (b) Solar light driven (with an AM 1.5 air mass filter) photo-catalytic water reduction for H_2 generation of different samples.

With increasing amounts of Pt nanoparticles on GR-MSCs, the photocatalytic activity of GR-MSCs increased first then decreased. The highest photocatalytic activity was achieved with 0.74 wt% Pt loading. The sandwiched GR-MSCs with or without Pt showed the highest activity for photo-oxidation of phenol. In addition, MSCs, GR-MSCs and MSCs@GR loading with Pt showed higher photo-oxidation activity than samples without Pt. Moreover, the MSCs@GR with 0.377 wt% Pt loading shows the highest formation rate in the photocatalytic hydrogen generation and the photocatalyst without Pt loading shows no photocatalytic activity.

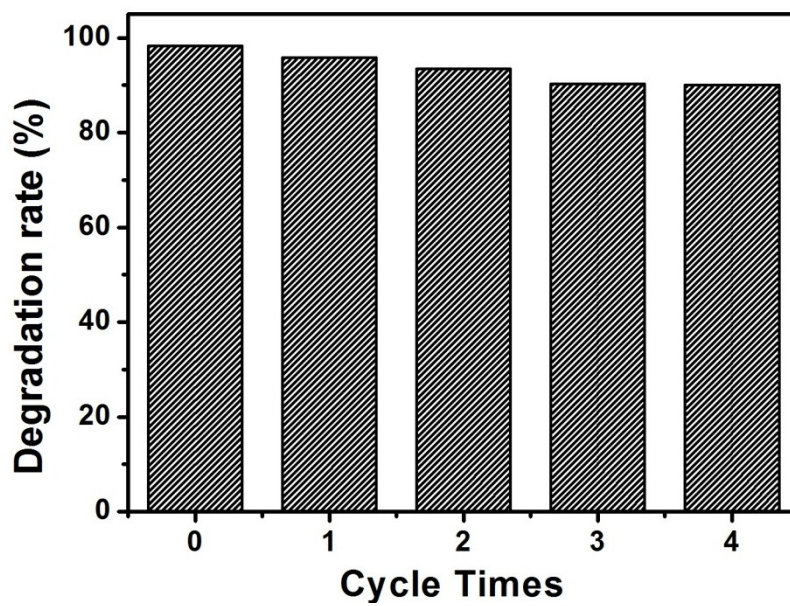


Fig. S18 Cycling tests of solar-driven photo-catalytic activity of sandwiched GR-MSCs for the degradation of phenol. A little decrease degradation rate with the increase of cycle times is induced by the loss of powders during every recycling of sample.

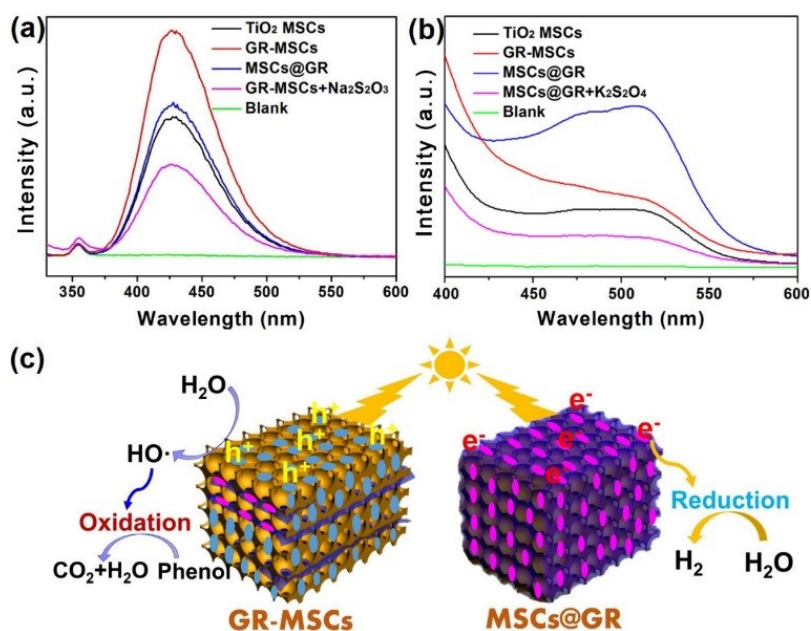


Fig. S19 (a) Photoluminescence spectra of terephthalic acid and terephthalic acid mixed with catalysts under the solar light irradiation for 30 min (“Blank” means the blank terephthalic acid solution). (b) UV-vis absorption spectra of ammonium ferric sulfate and Phen solution mixed with catalysts under the solar light irradiation for 60 min (“Blank” means the blank Fe³⁺/Phen solution). (c) The mechanism of the photo-oxidation of phenol on GR-MSCs and the photo-reduction of water for hydrogen evolution on MSCs@GR, respectively.

The holes-involved photooxidation reaction is the rate determining step on the GR-MSCs surface, explaining the comparatively poor catalytic photoreductive properties of the GR-MSCs tested here.

The presence of these exposed electrons on the surface of MSCs@GR is vital for the catalytic photo-reduction reaction, and this surface is responsible for the rapid catalytic splitting of water to H₂ observed here.

References:

1. W. Stöber, A. Fink and E. Bohn, *J. Colloid Interface Sci.*, 1968, **26**, 62-69.
2. B. Qiu, M. Xing and J. Zhang, *J. Am. Chem. Soc.*, 2014, **136**, 5852-5855.
3. W. S. Hummers and R. E. Offeman, *J. Am. Chem. Soc.*, 1958, **80**, 1339-1339.
4. M. Y. Xing, B. X. Yang, H. Yu, B. Z. Tian, S. Bagwasi, J. L. Zhang and X. Q. Gong, *J. Phy. Chem. Lett.*, 2013, **4**, 3910-3917.
5. X. Zheng, Q. Kuang, K. Yan, Y. Qiu, J. Qiu and S. Yang, *ACS Appl. Mater. Interfaces*, 2013, **5**, 11249-11257.
6. M. C. Yan, F. Chen, J. L. Zhang and M. Anpo, *J. Phys. Chem. B*, 2005, **109**, 8673-8678.
7. Q. Xiang, J. Yu and M. Jaroniec, *Nanoscale*, 2011, **3**, 3670-3678.
8. L. Xiao, D. Wu, S. Han, Y. Huang, S. Li, M. He, F. Zhang and X. Feng, *ACS Appl. Mater. Interfaces*, 2013, **5**, 3764-3769.
9. M. Xing, X. Li and J. Zhang, *Sci. Rep.*, 2014, **4**, 5493.
10. M. Xing, F. Shen, B. Qiu and J. Zhang, *Sci. Rep.*, 2014, **4**, 6341.
11. B. Qiu, Y. Zhou, Y. Ma, X. Yang, W. Sheng, M. Xing and J. Zhang, *Sci. Rep.*, 2015, **5**, 8591.
12. X. Wu, S. Yin, Q. Dong, B. Liu, Y. Wang, T. Sekino, S. W. Lee and T. Sato, *Sci. Rep.*, 2013, **3**, 2918.
13. J. Yu, G. Dai, Q. Xiang and M. Jaroniec, *J. Mater. Chem.*, 2011, **21**, 1049-1057.
14. Y. Zhang, P. Xiao, X. Zhou, D. Liu, B. B. Garcia and G. Cao, *J. Mater. Chem.*, 2009, **19**, 948-953.
15. H. Zhang, X. Lv, Y. Li, Y. Wang and J. Li, *ACS Nano*, 2009, **4**, 380-386.
16. S. Sakthivel and H. Kisch, *Angew. Chem. Int. Ed.*, 2003, **42**, 4908-4911.
17. J. Yang, H. Bai, Q. Jiang and J. Lian, *Thin Solid Films*, 2008, **516**, 1736-1742.
18. X. Zhao, T. Xu, W. Yao, C. Zhang and Y. Zhu, *Appl. Catal., B*, 2007, **72**, 92-97.